

Lense-Thirring Acoustic Black Holes : Shadows and Light

Anas El Balali¹ , and Alessio Marrani²

¹*Département de physique, Équipe des Sciences de la matière et du rayonnement, ESMaR*

Faculté des Sciences, Université Mohammed V de Rabat, Rabat, Morocco

²*Centre for Mathematics and Theoretical Physics, University of Hertfordshire, AL10 9AB Hatfield, UK*

E-mail: anas.elbalali@gmail.com, a.marrani@herts.ac.uk

ABSTRACT: We introduce the *Lense-Thirring Acoustic Black Hole* (LTABH), motivated by the relevance of analogue models for black holes embedded in various physical systems, such as the cosmological microwave background or quantum superfluids. We investigate the LTABH spacetime geometry, showing that the roots of the metric function determine a partition of the spacetime into four regions, depending on the acoustic parameter ξ (whereas the dependence vanishes for the rotation parameter a); on the other hand, the parameter a turns out to affect the critical radii associated to the maxima of the effective potential. All in all, both the acoustic sphere radius r_{as} and the photon sphere radius r_{ps} , respectively giving rise to the acoustic shadow R_{as} and to the optical shadow R_s , depend on ξ and a . More precisely, the rotation parameter a is more relevantly affecting R_s (through a right shift), while R_{as} retains its circular shape. For what concerns the acoustic parameter, we notice that the higher ξ is, the larger the size of both shadows. All of these results are confirmed through a detailed analysis of the distortions and of the shadows radii. Moreover, by deriving the magnitude of the precession frequency Ω , we observe that it significantly increases near the acoustic horizons, both in the extremal and in the non-extremal cases, which implies that the Lense-Thirring (frame dragging) effect, which can be traced back to ξ itself, becomes important near such regions. On the other hand, we also show that there are regions of the LTABH spacetime in which Ω vanishes, suggesting that therein possible probe particles would not be affected by the frame dragging at all. Finally, we derive the deflection of the light near the LTABH.

Keywords: Black hole analogues, Lense-Thirring acoustic black holes, Shadows, Distortion, Frame-dragging effect, Light deflection.

Contents

1	Introduction	1
2	Notation and Conventions	4
3	Review of Lense-Thirring acoustic black hole solution	4
4	Geometrical analysis	7
5	Shadows and null geodesics	9
5.1	General approach	9
5.2	Photon and acoustic spheres	11
5.3	Shadow forms	13
6	Lense-Thirring effect and precession	17
6.1	Mathematical Framework	17
6.2	Graphics and results	18
7	Deflection angle	20
8	Conclusions	22
A	On the placement of critical radii	24
B	The matrix $\mathcal{G}_{\mu\nu}$	25

1 Introduction

In Einstein’s theory of General Relativity, the presence of matter in the universe dictates how the spacetime shapes, as described by Einstein’s field equations [1]. Among the solutions to these equations, we find *black holes*. These objects are the result of the gravitational collapse of massive stars, at the end of their life cycle [2, 3]. Such a phenomenon leads to the formation of a *singularity*, surrounded by the event horizon, ‘the sphere of no return’. Black holes are therefore characterized by a very intense gravity that influences the surrounding spacetime, and which may thus lead to interesting optical phenomena. Indeed, it can be shown that black holes can act as a lens, causing the deflection of light (*gravitational lensing*) [4–11]. From another perspective, the so-called *black hole shadow* is also a consequence of the immense gravitational pull of these objects [12–17].

Furthermore, black holes exhibit thermodynamic properties such as the entropy, the temperature, and most importantly the Hawking radiation, in which quantum effects are

responsible for the black hole to emit radiation and slowly evaporate [18–25]. Along this and other research venues, the study of black holes keep providing remarkable insights on the unification of quantum mechanics and gravity [26–30]. Black holes have also played an important role in the understanding of gravitational waves : the detection of *GW 150914* published by LIGO and Virgo Collaboration has marked the first gravitational wave detection resulting from the merger of a binary black hole system [31]. It should also be recalled that imaging by the Event Horizon Telescope have provided an undeniable evidence of the existence of black holes themselves [32–39]. Such discoveries and unprecedented advances in the observation of black holes have aroused the interest of physicists around the world leading to a relentless and ever growing research activity.

Notwithstanding such ground-breaking results in the field of black hole physics, the experimental detection of the black hole features is still subject to limiting technical limitations. This can be regarded as one of the motivations which led to the birth of a new field of research in gravity, the so-called *analogue gravity*, aiming at mimicking gravitational phenomena in the laboratory; needless to say, analogies have been constantly playing a key role in mathematics and physics since they have offered new perspectives and simplifications of complex ideas. In particular, it is here worth remarking that, through table top experiments, analogue gravity established key connections between rotating black holes and the Hawking radiation. This was firstly reported in the seminal paper by Unruh [40], in which hydrodynamical flows were used to mimic some proprieties of black holes. In this framework, sound waves which are trapped inside a horizon led to the introduction of the name *acoustic black hole* or *dumb hole*. All in all, it has been argued that *any* fluid can ultimately give birth to an acoustic black hole, if it moves faster than the local sound velocity within a spherical surface [41–44]. Black hole analogues have been investigated within a wide range of classical and quantum systems; just to cite a few, gravity waves [45], water [46], ‘slow’ light [47–49], optical fibers [50], and electromagnetic waveguides [51]. Other models exhibiting promising features include the superfluid helium II [52], atomic Bose-Einstein condensates [53], and one-dimensional Fermi-degenerate non-interacting gases [54]. For further detail and a quite complete list of references, we address the interested reader to the comprehensive review [55].

Acoustic black holes have long been the subject of many studies. In a thermodynamical framework, Hawking-like radiation emitted by acoustic black holes has been successfully detected and studied in [56–58], and entropy of acoustic black holes has also been investigated in a number of studies [59–63]. More insights were gained by focussing on two-dimensional systems [64, 65], in which the investigation of the Bose-Einstein condensates provided an analogue of the Bekenstein-Hawking entropy [66]. While in [67] the entanglement entropy of acoustic black holes was investigated, the relation between the area of the acoustic black hole event horizon and the entropy has been the subject of [68]. Theoretically, the consideration of relativistic Gross-Pitaevski and Yang-Mills theories led to the embedding of the acoustic black hole into a curved background [69]; for instance, in [70] an acoustic black hole solution was related to a black *D*3-brane. Moreover, the investigation of such black hole analogues in the Abelian Higgs model led to the discovery of a relativistic acoustic black hole solution in Minkowski spacetime [41, 71].

An interesting property of acoustic black holes goes under the name of *acoustic shadow* : it can be regarded as the acoustic analogue of the optical shadow of a black hole that has been captured by the EHT collaboration, and it has been studied in a variety of backgrounds and contexts; see e.g. [72, 73]. The deflection angle has also been scrutinised in proximity of an acoustic black hole, in [74, 75]. At any rate, realistic models of acoustic black holes must necessarily include rotation : this is one of the motivations of [76], in which a slowly rotating solution has been constructed and investigated. In this framework, the interest of the analogue gravity approach towards the relativistic Gross-Pitaevskii theory as well as towards Yang-Mills (and thus, non-Abelian) gauge theories relies on a number of reasons; here, we will list three of them. Firstly, realistic models of astrophysical black holes include the embedding into the cosmological microwave background, and this makes the acoustic black holes natural candidates to be investigated in this venue [69]. Secondly, the relativistic and transonic accretion disks, surrounding supermassive black holes at the center of galaxies, serve as unique examples of analogue gravity models present in nature [77–80]. Thirdly, one should recall that black holes may also be surrounded by some quantum superfluids whose condensation can generally give rise to analogue gravitational phenomena; for instance, such fluids have been proposed to determine also dark matter phenomenology [81].

Motivated by this wealth of facts and results, it is our belief that acoustic black holes deserve further investigation, and they ultimately have a chance to be detected in reality. By taking advantage of a slowly rotating solution at hand, we aim at investigating more realistic frameworks, in which both phonon and photons can propagate in the corresponding spacetime.

In this work, we will present a detailed investigation of the impact of the rotation parameter on the slowly rotating and curved acoustic black hole. In particular, we will study the partition of the black hole geometry into different regions, depending on the acoustic parameter itself. By considering the null geodesics of the corresponding spacetime, we will gain insights about the behavior of the shadows and the corresponding distortion. Furthermore, we will study the Lense-Thirring effect, responsible for the frame dragging of rotating black holes. *Last but not least*, we will provide a careful analysis of the deflection angle, by exploiting the Gauss-bonnet method ¹.

The plan of the paper is as follows. Sec. 3 reviews of the slowly rotating acoustic black hole solution, whose geometry is analyzed in Sec. 4. Sec. 5 is then devoted to the study of the shadow and of the null geodesics of the black hole. We will define an *effective potential* as a function of the relevant black hole parameters, and we will study its critical points in an analytic and graphical way, focussing on the emergence of various critical radii. In this framework, we will investigate the shadows as parametric functions, and discuss their features. The subsequent Secs. 6 and 7 will be devoted to the analysis of the frame dragging effect, and to deflection of light around an acoustic black hole, respectively. Finally, in Sec. 8 we will summarize our results, provide remarks and an outlook to further developments. Two appendices conclude the paper : in App. A the placement of the aforementioned

¹In this work, we use dimensionless units, i.e. $c = G = 1$.

critical radii is discussed, whereas in App. B the explicit, lengthy expression of a matrix relevant for the LTABH metric is reported.

2 Notation and Conventions

In this paper, we adopt the following notations

Table 1: List of symbols in the paper

Symbol	Description
c_s	The speed of sound in the acoustic medium
M	The mass parameter of the non-acoustic case
a	The rotation parameter
ξ	The acoustic parameter
r_H	The horizon radius
r_{ac-}	The inner acoustic critical radius
r_{ac+}	The outer acoustic critical radius
r_{ac}	The acoustic critical radius in the extremal case ($\xi = 4$)
E	The particle's energy
L	The particle's angular momentum
\mathcal{K}	The separation constant
r_{ps}	The photon sphere radius in the acoustic case
r_{as}	The acoustic sphere radius
r_{ph}	The photon sphere radius in the non-acoustic case
η, ζ	The impact parameters
R_s	The shadow radius
R_{as}	The acoustic shadow radius
δ_s	The deformation of the apparent shadow
δ_{as}	The deformation of the acoustic shadow
K^α	The Killing vector
Ω	The Lense-Thirring precession frequency
$K_{\mathcal{G}}$	The Gaussian optical curvature

3 Review of Lense-Thirring acoustic black hole solution

In this part of the paper, we review the procedure to derive a slowly rotating acoustic black hole solution. In order to establish this solution, we follow the approach outlined in paper [76]. Indeed, within the framework of analogue gravity, the Lagrangian of relativistic Gross-Pitaevskii (GP) theory of a complex scalar field φ is written as

$$\mathcal{L} = g^{\mu\nu} \partial_\mu \varphi^* \partial_\nu \varphi - m^2 \varphi^* \varphi + \frac{b}{2} (\varphi^* \varphi)^2, \quad (3.1)$$

which yields the following action

$$S = \int d^4x \sqrt{-g} \left(|\partial_\mu \varphi|^2 - m^2 |\varphi|^2 + \frac{b}{2} |\varphi|^4 \right), \quad (3.2)$$

where b represents a coupling constant and m is a parameter that depends on the Hawking-Unruh temperature T of the resulting acoustic solution carrying information about the black hole and the acoustic metric. It is worth noting that such a parameter can be expressed as $m^2 \sim T - T_c$ with T_c being the critical temperature where phase transitions can occur. The variation of the action, can provide the motion of φ which is described by the following equation

$$\square \varphi + m^2 \varphi - b |\varphi|^2 \varphi = 0. \quad (3.3)$$

The acoustic black hole solution of such a theory can be derived by perturbing the complex scalar field φ around the spacetime background. Such a field can propagate in a fixed background spacetime described by the metric

$$ds^2 = -g_{tt} dt^2 + g_{rr} dr^2 + g_{\theta\theta} d\theta^2 + g_{\phi\phi} d\phi^2 + 2g_{t\phi} dt d\phi. \quad (3.4)$$

It is worth recalling that such a metric form has been chosen to align with a slowly rotating black hole, similar to the **Lense-Thirring Black Hole (LTBH)**, which will be introduced later [82]. Indeed, the slowly rotating approximation assumes that higher-order terms of the rotation parameter a , which is embedded in the component $g_{t\phi}$, are negligible. The scalar field φ can be expressed as a function of the fluid density $\rho = \rho_0 + \epsilon \rho_1$ and the phase $\vartheta = \vartheta_0 + \epsilon \vartheta_1$ as follows

$$\varphi = \sqrt{\rho(\vec{x}, t)} \exp(i\vartheta(\vec{x}, t)). \quad (3.5)$$

In the hydrodynamic or Thomas-Fermi limit the quantum pressure $P_Q = \frac{\square \sqrt{\rho}}{\sqrt{\rho}}$ can be neglected in front of the quantities $m^2, b\rho_0, v^\mu v_\mu$. Thus, replacing φ in equation (3.3), one finds the background fluid density leading order equation which reads

$$b\rho_0 \equiv 2c_s^2 = m^2 - g^{\mu\nu} v_\mu v_\nu, \quad (3.6)$$

where (ρ_0, ϑ_0) and (ρ_1, ϑ_1) are associated to the background solution in fixed spacetime and to fluctuations respectively, while c_s is the speed of sound. It is worth noting that the background four-velocity v_μ has been defined as $v_\mu = (-\partial_t \vartheta_0, \partial_i \vartheta_0)$. In order to determine the relativistic wave equation, we use the continuity equation that reads as

$$\nabla_\mu (\rho v^\mu) = \nabla_\mu (\rho_0 v_0^\mu) + \epsilon \nabla_\mu (\rho_0 \partial^\mu \vartheta_1 + \rho_1 v_0^\mu) = 0, \quad (3.7)$$

where $\nabla_\mu (\rho_0 v_0^\mu) = 0$ is associated to the background continuity equation and the first order term gives the linearized continuity equation for fluctuations

$$\nabla_\mu (\rho_0 \partial^\mu \vartheta_1 + \rho_1 v_0^\mu) = 0. \quad (3.8)$$

At subleading order in ϵ [83], the decomposition of the scalar field φ when replaced in equation of motion of the scalar field (3.3) leads to

$$\rho_1 = -\frac{2}{b} v_0^\mu \partial_\mu \vartheta_1. \quad (3.9)$$

Replacing in equation (3.8), one gets

$$\nabla_\mu \left(\rho_0 g^{\mu\nu} - \frac{2}{b} v_0^\mu v_0^\nu \right) \partial_\nu \vartheta_1 = 0. \quad (3.10)$$

As a result, the effective metric can be taken as

$$\mathcal{G}^{\mu\nu} \propto \rho_0 g^{\mu\nu} - \frac{2}{b} v_0^\mu v_0^\nu. \quad (3.11)$$

Finally, the relativistic wave equation that dictates the propagation of the phase fluctuations is

$$\frac{1}{\sqrt{-\mathcal{G}}} \partial_\mu \left(\sqrt{-\mathcal{G}} \mathcal{G}^{\mu\nu} \partial_\nu \vartheta_1 \right) = 0. \quad (3.12)$$

As a results, one could extract from such equation the effective metric $\mathcal{G}_{\mu\nu}$ which is given in App. B.

Assuming that $v_t \neq 0$, $v_r \neq 0$, $v_\theta = 0$, $v_\phi = 0$ and $g_{rr}g_{tt} = -1$, and using the following coordinate transformaions

$$dt \rightarrow dt + \frac{v_r v_t}{g_{tt} (c_s^2 - v_i v^i)} dr, \quad (3.13)$$

$$d\phi \rightarrow d\phi - \frac{g_{t\phi} (c_s^2 - v_t v^t) v_t v_r}{g_{\phi\phi} g_{tt} (c_s^2 - v_\mu v^\mu) (c_s^2 - v_r v^r)} dr, \quad (3.14)$$

we get the line element of a slowly rotating and curved acoustic black hole

$$ds^2 = c_s \sqrt{c_s^2 - v_\mu v^\mu} \left(\frac{c_s^2 - v_r v^r}{c_s^2 - v_\mu v^\mu} g_{tt} dt^2 + \frac{c_s^2}{c_s^2 - v_r v^r} g_{rr} dr^2 + g_{\theta\theta} d\theta^2 + g_{\phi\phi} d\phi^2 + 2 \frac{c_s^2 - v_t v^t}{c_s^2 - v_\mu v^\mu} g_{t\phi} dt d\phi \right). \quad (3.15)$$

In order to fully define such a spacetime, we identify the fluid four-velocity with the LTBH whose metric is written as

$$ds^2 = -f(r) dt^2 + \frac{dr^2}{f(r)} + r^2 d\theta^2 + r^2 \sin^2 \theta d\phi^2 - 2(1 - f(r)) a \sin^2 \theta dt d\phi, \quad (3.16)$$

where the metric function is

$$f(r) = 1 - \frac{2M}{r}, \quad (3.17)$$

and a is the rotation parameter [82]. Regarding the four-velocity, one can use the equation (3.6) and rescale in terms of natural units of $2c_s^2$ as follows

$$\tilde{v}_\mu \rightarrow \frac{v_\mu}{\sqrt{2c_s^2}}, \quad (3.18)$$

which gives

$$\tilde{v}_\mu \tilde{v}^\mu = \frac{m^2}{2c_s^2} - 1. \quad (3.19)$$

Thus, for $m^2 \rightarrow 0$ in the limit of the critical temperature T_c , we get

$$v_\mu v^\mu = -1. \quad (3.20)$$

The escape velocity of an observer who remains stationary at the radial point r can be associated with the radial component of the fluid four-velocity. In this way, we have

$$v_r \sim \sqrt{(1 - f(r))\xi}, \quad (3.21)$$

where ξ represents an acoustic parameter that constrains the acoustic event horizon to be outside the event horizon of the black hole. On another hand, we can write

$$v_\mu v^\mu = g^{tt} v_t^2 + g^{rr} v_r^2 = -\frac{v_t^2}{f(r)} + f(r)v_r^2. \quad (3.22)$$

With $v_\mu v^\mu = -1$, equation (3.22) gives

$$v_t = \sqrt{f(r) + (1 - f(r))f(r)^2\xi}. \quad (3.23)$$

Finally, the metric of equation (3.15) can be rewritten as

$$ds^2 = -F(r)dt^2 + \frac{dr^2}{F(r)} + r^2d\theta^2 + r^2\sin^2\theta d\phi^2 - 2(1 - F(r))a\sin^2\theta dt d\phi, \quad (3.24)$$

where the acoustic metric functions $F(r)$ is given by

$$F(r) = f(r)[1 - f(r)(1 - f(r))\xi]. \quad (3.25)$$

For simplicity reasons, the speed of sound has been fixed, i.e $c_s^2 = 1/\sqrt{3}$. It is worth noticing that, the escape velocity v_r in equation (3.21) implies that the parameter ξ must be strictly positive. Besides, when the acoustic parameter $\xi \rightarrow 0$, we recover the LTBH while when $\xi \rightarrow \infty$, i.e $v_r \rightarrow \infty$, the entire spacetime is covered by the LTABH.

The spacetime geometry of a LTABH is described by equations (3.24), (3.25), and $f(r) = 1 - 2M/r$. Such scenario offers valuable insight which deserves further investigation. In what follows, we analyse the geometry of the this solution, discuss the roots of the acoustic metric function $F(r)$ in terms of the acoustic parameter ξ and derive the shadow equation. We also investigate the critical radii involved in the acoustic case and shed light on the frame dragging effect and the deflection angle of the present solution.

4 Geometrical analysis

The considered solution is similar to the LTBH since the event and acoustic horizons do not depend on the rotation parameter a . Indeed, by solving $F(r) = 0$ three solutions are derived, which are

$$r_H = 2M, \quad r_{ac-} = M\left(\xi - \sqrt{\xi(\xi - 4)}\right), \quad r_{ac+} = M\left(\xi + \sqrt{\xi(\xi - 4)}\right), \quad (4.1)$$

which are represented with the metric function $F(r)$ in figure (1).

By analysing the roots of the metric function $F(r)$, we remark that the inner acoustic horizon r_{ac-} and the outer acoustic horizon r_{ac+} exist only if $\xi > 4$, while when $\xi = 4$, we have $r_{ac-} = r_{ac+} = 4M$ which corresponds to the extremal case of the slowly rotating

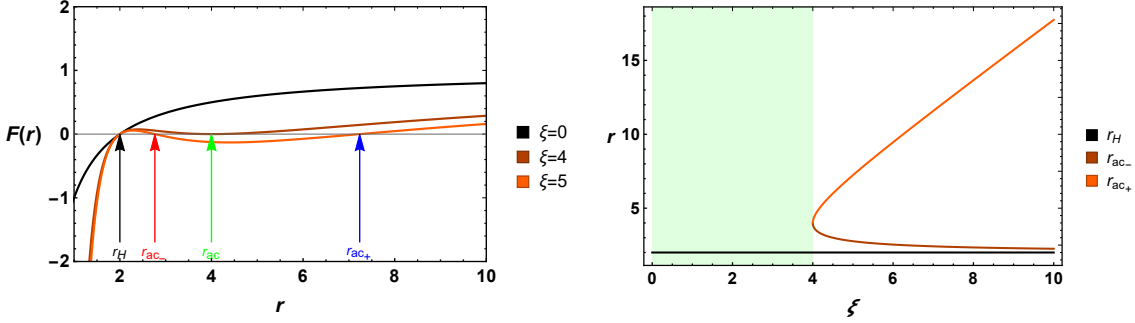


Figure 1: Left: Profile of the metric function $F(r)$ with its roots for different values of the parameter ξ . Right: The roots as a function of the parameter ξ . The green region represents the non allowed values of ξ , i.e $\xi < 4$. We take $M = 1$.

acoustic black hole. In the right side of figure (1), we notice that the solutions associated with the acoustic aspect of the black hole r_{ac_-} and r_{ac_+} are larger than the horizon radius r_H . Moreover, it is clear that the inner acoustic horizon r_{ac_-} converges to the value $2M$ as the acoustic parameter ξ increases, while the outer acoustic horizon r_{ac_+} diverges to infinity for higher values of ξ . This shows that as the acoustic parameter increases, no sound wave could escape the spacetime, while other particles can be absorbed by the event horizon. For the particular value of $\xi = 4$, we obtain the extremal case which is characterized by only one acoustic horizon. It is worth mentioning that the positive values of $F(r)$ indicates that the fluid velocity is less than the speed of sound which means that the sound waves could move freely in this spacetime region. In contrast, sound waves in a region with a negative $F(r)$ will be confined and unable to be heard by outside observers.

Interestingly, for $\xi > 4$ and an observer in the region $r_H < r < r_{ac_-}$, the radius r_{ac_-} could be regarded as the white hole's acoustic horizon. In particular, the fluid flow is approaching the observer in the subsonic area $r_H < r < r_{ac_-}$ from the supersonic region ($r_{ac_-} < r < r_{ac_+}$), having crossed the horizon (r_{ac_-}). It is fair to consider r_{ac_-} to be the horizon of the acoustic white hole for this observer because, as a result, sound waves in the subsonic zone cannot travel against the fluid flow into the supersonic region, whereas the opposite is permitted. Furthermore, the behavior of the metric function $F(r)$ varies depending on r_{ac_-} and r_{ac_+} as it can be noticed from the left plot of figure (1). Indeed, $F(r) > 0$ in the region of $r < r_{ac_-}$, while $F(r) < 0$ in the region of $r > r_{ac_-}$, suggesting that the inner acoustic horizon share some characteristics with the charged black hole's Cauchy horizon. Conversely, the metric function near the outer acoustic horizon exhibits behavior similar to the black hole's event horizon, with $F(r) < 0$ for $r < r_{ac_+}$ and $F(r) > 0$ for $r > r_{ac_+}$.

Based on the aforementioned factors, we can conclude that the acoustic black hole is characterized by four regions.

- Region I with $r < r_H$: inside the LTABH black hole, where neither light nor sound waves may escape.

- Region II, where $r_H < r < r_{ac_-}$, is the area where light and sound waves can exit but are invisible to observers outside of it.
- Region III with $r_{ac_-} < r < r_{ac_+}$, whereas the sound wave cannot escape from but light can.
- Region IV with $r > r_{ac_+}$, both the light and sound waves can escape.

For the particular extremal case of $\xi = 4$, $r_{ac_-} = r_{ac_+} = r_{ac}$, we are left with only three regions and the function $F(r)$ is negative only in region I.

5 Shadows and null geodesics

In this section, we analyse the effective potential behavior of the slowly rotating acoustic black hole described by the metric (3.24). With the help of null geodesics, we derive relevant regions in which the effective potential has a particular behavior. Moreover, we investigate the shadows in the vicinity of an acoustic black hole and illustrate its behavior.

5.1 General approach

Studying the null geodesics is necessary in order to inspect the evolution of the massless particles surrounding the black hole under consideration [84]. In order to do so, we use the following Hamilton-Jacobi equation

$$\frac{\partial S}{\partial \tau} = -\frac{1}{2}g^{\mu\nu}\frac{\partial S}{\partial x^\mu}\frac{\partial S}{\partial x^\nu}, \quad (5.1)$$

where τ denotes the affine parameter of the null geodesic and the Jacobi action can be separated in the following manner

$$S = \frac{1}{2}m_0^2\tau - Et + L\phi + S_r(r) + S_\theta(\theta). \quad (5.2)$$

The mass m_0 is equal to zero for the class of massless particles. The particles energy and angular momentum are denoted by E and L , respectively, and the functions $S_r(r)$ and $S_\theta(\theta)$ only depend on r and θ , respectively. The following equation is obtained using the slow rotation metric (3.24) by substituting the Jacobi action (5.2) into the Hamilton-Jacobi equation (5.1)

$$0 = -F(r)^{-1}\left(\frac{\partial S}{\partial t}\right)^2 + \frac{1}{r^2}\left(\frac{\partial S}{\partial \phi}\right)^2 - 2a\sin^2\theta\frac{(1-F(r))}{r^2F(r)}\left(\frac{\partial S}{\partial t}\right)\left(\frac{\partial S}{\partial \phi}\right) \quad (5.3)$$

$$+ F(r)\left(\frac{dS_r}{dr}\right)^2 + \frac{1}{r^2\sin^2\theta}\left(\frac{dS_\theta}{d\theta}\right)^2 + \mathcal{O}(a^2). \quad (5.4)$$

Additional computations and reductions yield

$$r^4F(r)\left(\frac{dS_r}{dr}\right)^2 = \frac{E^2r^4}{F(r)} + 2aELr^2\frac{(1-F(r))}{F(r)} - r^2(L^2 + \mathcal{K}), \quad (5.5)$$

$$\frac{1}{\sin^2\theta}\left(\frac{dS_\theta}{d\theta}\right)^2 = \mathcal{K} - 2aEL\frac{(1-F(r))}{F(r)}\cos^2\theta. \quad (5.6)$$

where \mathcal{K} represents the separation constant. We derive the whole set of equations characterizing the photon motion using the definition of the canonically conjugate momentum $p_\mu = g_{\mu\nu} \frac{dx^\nu}{d\tau}$. In this way, we get

$$r^2 \frac{dt}{d\tau} = \frac{Er^2}{F(r)} - aL \frac{(1 - F(r))}{F(r)} \sin^2 \theta, \quad (5.7)$$

$$r^2 \frac{dr}{d\tau} = \sqrt{R(r)}, \quad (5.8)$$

$$r^2 \frac{d\theta}{d\tau} = \sqrt{\Theta(\theta)}, \quad (5.9)$$

$$r^2 \frac{d\phi}{d\tau} = L + aE \frac{(1 - F(r))}{F(r)} \sin^2 \theta. \quad (5.10)$$

where the formulas of $R(r)$ and $\Theta(\theta)$ are

$$R(r) = E^2 r^4 + 2aELr^2 (1 - F(r)) - r^2 F(r)(L^2 + \mathcal{K}), \quad (5.11)$$

$$\Theta(\theta) = \mathcal{K} \csc^2 \theta - 2aEL \frac{(1 - F(r))}{F(r)} \cot^2 \theta. \quad (5.12)$$

An appropriate method for examining the geometric shapes of the shadow and to derive the acoustic and photon sphere would be to take into account the effective potential, which takes the following form

$$V_{eff}(r) = - \left(\frac{dr}{d\tau} \right)^2 = -E^2 + \frac{2aEL}{r^2} (F(r) - 1) + \frac{F(r)}{r^2} (L^2 + \mathcal{K}). \quad (5.13)$$

It is worth remarking that the obtained potential matches the regular LTBH black hole when $\xi = 0$, i.e $F(r) = f(r) = 1 - \frac{2M}{r}$. We present the following impact factors in order to investigate the geometrical shape of the shadow in the slowly rotating regime

$$\zeta = \frac{L}{E}, \quad \eta = \frac{\mathcal{K}}{E^2}. \quad (5.14)$$

These two impact parameters are used to rewrite the function $R(r)$ given in (5.11) as

$$R(r) = E^2 (r^4 + 2a\zeta r^2 (1 - F(r)) - r^2 F(r)(\zeta^2 + \eta)). \quad (5.15)$$

The following conditions allow for the direct derivation of the critical unstable circular orbits

$$R(r)|_{r_i} = 0, \quad \frac{dR(r)}{dr}|_{r_i} = 0. \quad (5.16)$$

Thus, using (5.15) and (5.16), we obtain the impact parameters η and ζ , which are

$$\zeta = \frac{r(rF'(r) - 2F(r))}{2aF'(r)}, \quad (5.17)$$

$$\eta = \frac{r(8a^2F'(r) - (rF'(r) - 2F(r))((r^2 - 4a^2)F'(r) - 2rF(r)))}{4a^2F'^2}. \quad (5.18)$$

The shadow is then governed by the following equation

$$R_s^2 = \zeta^2 + \eta. \quad (5.19)$$

5.2 Photon and acoustic spheres

In this part of the paper, we use the equations established in the previous section to inspect the different regions that can be obtained from the effective potential of equation (5.13). To examine its behaviors and determine its maximum values, we illustrate such quantity versus r for different values of the spin parameter a and the acoustic parameter ξ in figure (2).

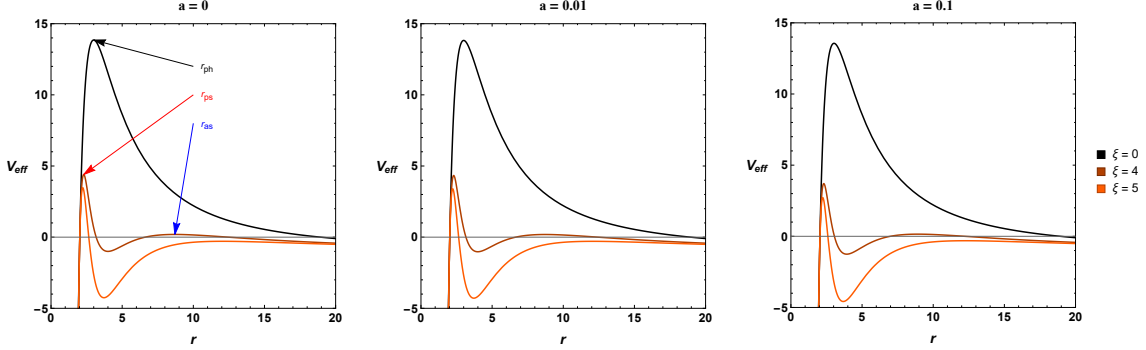


Figure 2: Effective potential for different values of the acoustic parameter ξ and different values of the rotating parameter a . The black curve is associated to the LTBH black hole. We take $M = 1$, $E = \mathcal{K} = 1$ and $L = 20$.

From such a figure, we remark that the effective potential has different extrema when the acoustic parameter $\xi \geq 4$. The most relevant are the two maximum which are associated to the photon sphere radius r_{ps} and to the acoustic sphere r_{as} while such a behavior vanishes when $\xi = 0$ where only one maximum associated to the photon sphere radius r_{ph} is present. Such radii are represented in the left panel of figure (2) for the case of $a = 0$. With these plots in hand, it can be observed that the photon sphere radius r_{ps} decreases when higher values of ξ are considered, while the opposite behavior is observed for the acoustic sphere radius r_{as} . From the three different panels, we can deduce that the higher the rotation parameter a gets, the larger these radii are. To investigate the extrema of the effective potential, we derive the later and solve the following equation

$$V'_{eff}(r)|_{r=r_i} = \frac{4aEL - (2F(r) - rF'(r)) (2aEL + \mathcal{K} + L^2)}{r^3} = 0. \quad (5.20)$$

By defining $(2aEL + \mathcal{K} + L^2) = A$, $4aEL = B$ and explicitating the factor $(2F(r) - rF'(r))$, we obtain

$$\frac{A (40M^3\xi - 32M^2\xi r + 6M(\xi + 1)r^2 - 2r^3) + Br^3}{r^6} = \frac{-\textcolor{blue}{e}r^3 + br^2 - cr + d}{r^6} = 0, \quad (5.21)$$

where $\textcolor{blue}{e} = 2A - B$, $b = 6AM(\xi + 1)$, $c = 32AM^2\xi$, $d = +40AM^3$. It can be shown that such

an equation admits three solutions that are

$$r_1 = \frac{b}{3e} + \frac{2^{1/3} (3ec - b^2)}{3e (X)^{1/3}} - \frac{(X)^{1/3}}{3\sqrt[3]{2}e}, \quad (5.22)$$

$$r_2 = \frac{b}{3e} - \frac{(1 + i\sqrt{3}) (3ec - b^2)}{3 2^{2/3}e (X)^{1/3}} + \frac{(1 - i\sqrt{3}) (X)^{1/3}}{6 2^{1/3}e}, \quad (5.23)$$

$$r_3 = \frac{b}{3e} - \frac{(1 - i\sqrt{3}) (3ec - b^2)}{3 2^{2/3}e (X)^{1/3}} + \frac{(1 + i\sqrt{3}) (X)^{1/3}}{6 2^{1/3}e}, \quad (5.24)$$

where

$$X = \sqrt{(27e^2d - 9ebc + 2b^3)^2 - 4(b^2 - 3ec)^3} - 27e^2d + 9ebc - 2b^3. \quad (5.25)$$

To fully identify these quantities further investigation should be carried. Indeed, to visualise the critical radii behaviors, we plot the three roots of the effective potential derivative against the acoustic parameter ξ in figure (3). With these figures and after a numerical analysis, it appears that when $\xi = 0$ the solution r_2 can be associated to the photon sphere radius r_{ph} while for $\xi \geq 4$ such a solution is associated to the acoustic sphere radius r_{as} .

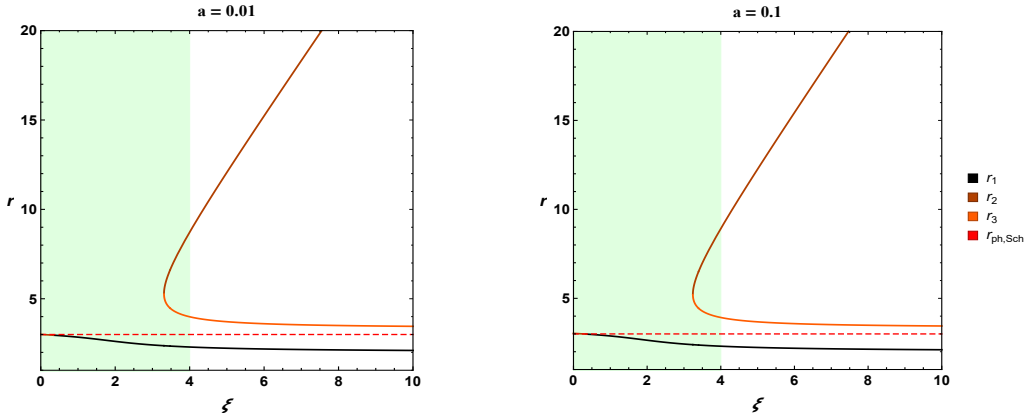


Figure 3: Roots of the effective potential derivative against the acoustic parameter ξ . The red dashed curve is associated to photon sphere radius of the LTBH black hole. We take $M = 1$, $E = \mathcal{K} = 1$ and $L = 20$.

To analyse each radius in detail, we first compute the effective potential and its derivative for a LTBH ($\xi = 0$)

$$V_{eff} = -\frac{4aELM + L^2(2M - r) + 2KM + E^2r^3 - Kr}{r^3}, \quad (5.26)$$

$$V'_{eff} = \frac{12aELM + L^2(6M - 2r) + 6KM - 2Kr}{r^4}. \quad (5.27)$$

The solution to $V'_{eff} = 0$, is given by $r_{ph} = M \left(\frac{6aEL}{K+L^2} + 3 \right)$. For the case where $a = 0$, it matches the Schwarzschild photon sphere $r_{ph} = 3M$. In this way, the LTABH can be linked

to the Schwarzschild black hole by turning off the acoustic parameter ξ and the rotation parameter a which results as follows $r_1 = 0$, $r_2 = r_{ph} = 3M$, $r_3 = 0$. At the same time, it can be seen from the plots that the radius r_2 plays another role when the value of the acoustic parameter $\xi \geq 0$. Actually, it is associated to the acoustic sphere radius r_{as} since its values are expected to be the largest. Seeing that r_3 corresponds to the minimum of the effective potential, such a radius will not be considered because it is not physically relevant. Finally, we have the solution r_1 which represents the photon sphere radius r_{ps} for $\xi \geq 4$ and have the lowest values compared to the other critical radii. Concerning the impact of the parameter a , its effect is barely visible.

From such an analysis, we expect the LTABH to be characterized by two shadows. The first, is the *optical shadow* $R_s(r_{ps})$ associated with the behavior of photons near the horizon while the second is the *acoustic shadow* $R_s(r_{as})$ that describes the characteristics of sound waves approaching the acoustic horizon.

5.3 Shadow forms

As we have previously mentioned, in the frame of a LTABH, the optical shadow surrounding the event horizon, which describes the visual boundary that light cannot escape from by viewers, and the acoustic shadow, which describes the audible boundary of the sound waves detected by static listeners, may coexist. In what follows, we derive the equation governing such aspects of the black hole where the photon-phonon interaction has been neglected to avoid complications. Using equations (5.17), (5.18) and considering that the observer is located at the equatorial plan ($\theta = \frac{\pi}{2}$), we illustrate the shadow radius denoted by R_s as a function of the acoustic parameter ξ in figure (4) for the different radii r_i derived from the previous section, with $i = 1, 2, 3$.

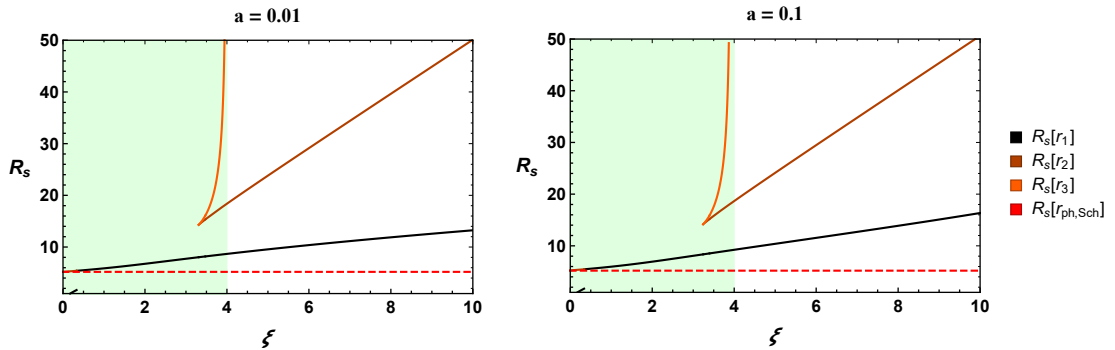


Figure 4: Shadow radius as a function of the effective potential extrema against the acoustic parameter ξ . The red dashed curve is associated to photon sphere radius of the LTABH black hole for which $R_s = 3\sqrt{3}M$. We take $M = 1$, $E = \mathcal{K} = 1$ and $L = 20$.

As expected, the behavior of the shadow radius $R_s(r_3)$ is not physically relevant since its values range in the green region where the values of the acoustic parameter ξ are not allowed. We also observe from such a figure that the shadow radius of the LTABH black hole coincide with $R_s(r_2)$ for the particular value of $\xi = 0$ proving that the root r_2 can

be associated with the photon sphere in such a case. When higher values of the acoustic parameter ξ are taken into consideration, we have two shadows. The acoustic shadow $R_s(r_{as}) := R_s(r_2)$ and the usual shadow $R_s(r_{ps}) := R_s(r_1)$. An interesting behavior arises from such a figure: indeed, we remark that increasing the rotating parameter a has a bigger impact on the shadow radius than the Acoustic shadow radius. This impact is also more visible for higher values of ξ .

The shadow geometrical shape is regulated by the permitted values of ζ and η . But a more precise method to visualize the shadow from a distance would be to utilise the celestial coordinates x and y defined by

$$x = \lim_{r_* \rightarrow \infty} \left(-r_*^2 \sin^2 \theta_0 \frac{d\phi}{dr} \right), \quad (5.28)$$

$$y = \lim_{r_* \rightarrow \infty} r_*^2 \frac{d\theta}{dr}, \quad (5.29)$$

where r_* is the distance between the black hole and the observer and θ_0 is associated to the inclination angle between the line rotational axis of the black hole and the observer line of sight [85]. As a function of the impact parameters, these two celestial coordinates can be written as

$$x = -\zeta \csc \theta_0, \quad (5.30)$$

$$y = \sqrt{\eta - \zeta^2 \cot^2 \theta_0}, \quad (5.31)$$

With the use of the celestial coordinates, we illustrate the regular and acoustic shadow at the equatorial plan in figure (5) for different values of ξ and a .

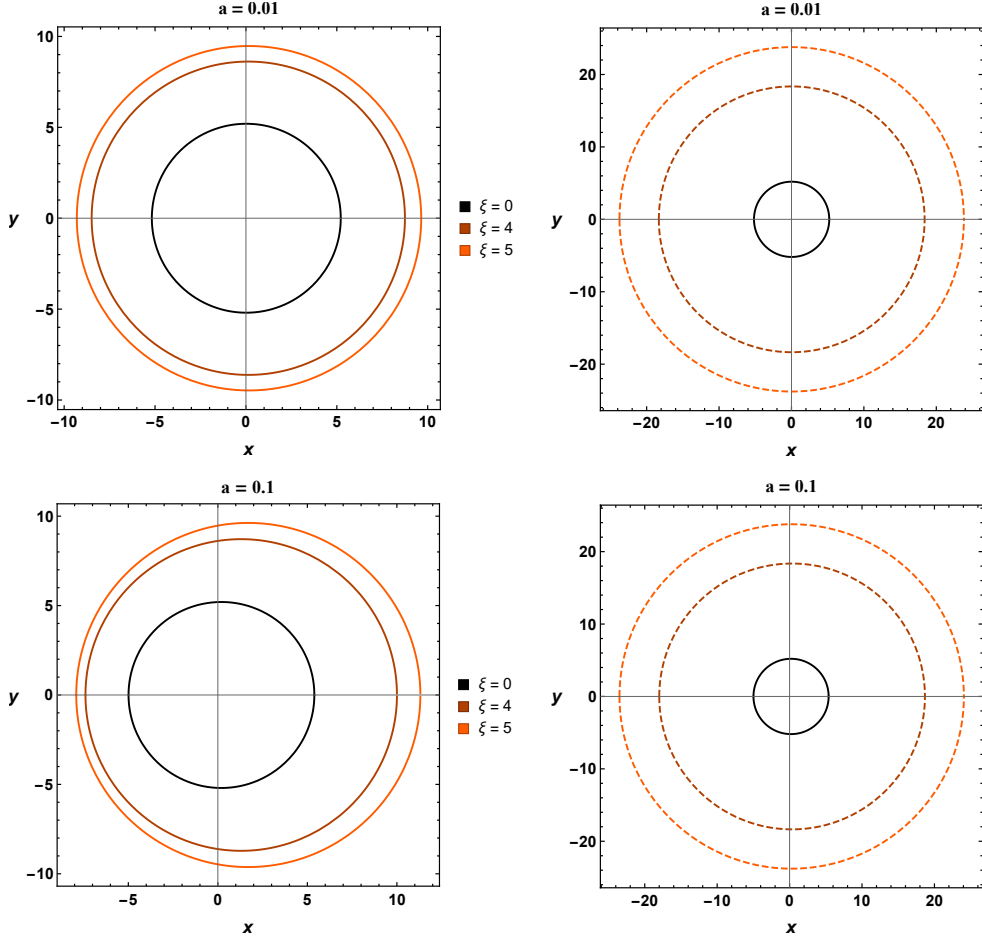


Figure 5: Left: Regular shadow $R_s(r_{ps})$. Right: Acoustic shadow $R_s(r_{as})$. We consider for these illustrations different values of the acoustic parameter ξ , the spin a and a fixed black hole mass ($M = 1$).

From such a figure, interesting features arises. Indeed, we observe that for low values of the rotating parameter a , both shadows are circular. In this case, increasing the value of the acoustic parameter ξ is associated to larger shadows. When the rotating parameter a is increased, we remark that the acoustic shadow (right plots) maintains the circular shape which proves that the acoustic shadow is barely affected by the rotation of the black hole. Concerning the regular shadow, the frame dragging effect shifts the shadows to the right side when a is increased. Such illustrations show that we must expect larger shadows in the case of acoustic black hole compared to other known black hole like Kerr, Reissner-Nördstrom or Schwarzschild.

To complete the essential building blocks associated with the optical behavior of this solution, an examination of the shadow size and shape is imposed. By examining these aspects, we can understand the geometric shadow behaviors, whether the regular or the acoustic one. This analysis is essential for a comprehensive overview of the underlying physical phenomena and the specific characteristics of the massive objects that generate these shadows, such as LTABH. To examine the geometric deformations of the two shadow

types, the visual and acoustic one, two essential parameters are generally used : (R_s, R_{as}) and (δ_s, δ_{as}) representing the size and the deformation of visual and acoustic shadows, respectively. The size of the shadow is specifically defined by three key points: the upper position (x_t, y_t) , the bottom position (x_b, y_b) and the circle reference point $(x_r, 0)$ associated with the non deformed geometry. The point where the deformed shadow circle intersects the horizontal axis is denoted $(x_i, 0)$. The distance between the reference point and the point of intersection, provides a quantifiable measure of the geometric deviation caused by the variation of the relevant parameters controlling the present solution. Consequently, the shadow radius $R_{s/as}$ and the deformation $\delta_{s/as}$ are approximately determined by the following expressions

$$R_{s/as} = \frac{(x_t - x_r)^2 + y_t^2}{x_t - x_r} \quad (5.32)$$

and

$$\delta_{s/as} = \frac{(x_i - x_p)}{R_{s/as}} \quad (5.33)$$

where x_r is the rightmost position of the circle. Based on these expressions, we can calculate the size and the geometrical deformation of the visual and acoustic shadows. Indeed, in table.(2), we report these quantities with respect to the spin and the acoustic parameter variations. A close examination show that the radius of the regular and the acoustic shadow increase with ξ for fixed values of the spin parameter. By fixing ξ , we can distinguish between the spin impact on the shadow radius and the acoustic radius. In fact, we observe that the quantity R_s increases while the quantity R_{as} undergoes a negligible change. Moreover, the acoustic shadow is bigger than the regular one for fixed values of the parameters a and ξ . This particularity could be linked to the fundamental differences in size between the radius of the photon sphere and the region of acoustic shadow formation. This means that sound waves can bypass objects more easily. Regarding the distortion parameter $\delta_{s/as}$, it is almost constant by varying ξ . By increasing such a parameter, we notice that the distortion decreases. In this regard, we remark a small difference in the distortion parameter by varying the spin. Besides, it can be observed that the spin has more impact on δ_s than δ_{as} .

	$a = 0.01$			$a = 0.1$		
	$\xi = 0$	$\xi = 4$	$\xi = 5$	$\xi = 0$	$\xi = 4$	$\xi = 5$
R_s	5.19	8.61	9.47	5.19	8.71	9.62
δ_s	1.45×10^{-4}	4.08×10^{-5}	2.7×10^{-4}	2.23×10^{-3}	1.78×10^{-3}	1.13×10^{-3}
R_{as}	5.19	18.35	23.78	5.19	18.35	23.78
δ_{as}	1.45×10^{-4}	1.89×10^{-5}	1.9×10^{-5}	2.23×10^{-3}	6.86×10^{-4}	2.56×10^{-4}

Table 2: Geometrical deformation of slowly rotating acoustic black hole by varying the spin and ξ parameters.

6 Lense-Thirring effect and precession

In this part of the paper, we study the frame-dragging effect (i.e., Lense-Thirring precession) of the LTABH on the spin of a test gyroscope. One of the key predictions of Einstein's general relativity is the Lense-Thirring precession, which has historically been the subject of enormous research efforts [86, 87]. The spin precession of a test gyroscope in the gravitational field of a spinning spherical body was first reported by Josef Lense and Hans Thirring in 1918. The Lense-Thirring precession effect can be used to anticipate the causal structures of the spacetime geometries. Consequently, it is crucial to understand the Lense-Thirring precession phenomenon in order to differentiate between the different black holes. In the following section, we review the mathematical description of the Lense-Thirring effect [88]. Then, we use the findings to analyse the frame-dragging in the vicinity of a LTABH.

6.1 Mathematical Framework

In the what follows, we examine a straightforward situation in which the gyroscopes are fixed at each point in space, and we look into how the precession frequency of the test gyroscope's spin varies as the spatial points move. The gyroscope moves along an integral curve $\gamma(t)$ of a timelike Killing vector field K since it is at rest in a stationary spacetime [89]. Then, the gyroscope's four-velocity u^α can be expressed in terms of K^α as follows

$$u^\alpha = \frac{1}{\sqrt{-K^\beta K_\beta}} K^\alpha. \quad (6.1)$$

In this way, one could express the four-velocity vector of the timelike curve $\gamma(\tau)$ as $u = \dot{\gamma}$, with u being tangent to $\gamma(\tau)$ and satisfying the condition $u^\mu u_\mu = -1$ and τ being the proper time. It is worth noting that the Fermi derivative component of any vector in the u -direction can be written as

$$u^\alpha F_\alpha X^\beta = u^\alpha \nabla_\alpha X^\beta - X^\alpha a_\alpha u^\beta + X^\alpha u_\alpha a^\beta, \quad (6.2)$$

where the acceleration is $a^\alpha = u^\beta \nabla_\beta u^\alpha$. Given the definition $e_\mu^\alpha e_{\nu\alpha} = \eta_{\mu\nu} = \text{diag}(-1, 1, 1, 1)$ in which the orthonormal frame $\{e_i\}$ ($i = 1, 2, 3$) is perpendicular to $e_0 = u$, we may write the components of the co-variant derivative in the direction of four-velocity u_α of the orthonormal basis as

$$u^\beta \nabla_\beta e_i^\alpha = e_i^\beta a_\beta u^\alpha + \omega_i^j e_j^\alpha, \quad (6.3)$$

with $\omega_i^j = u^\alpha \nabla_\alpha e_\beta^j e_\beta^\alpha$. With the help of the equations (6.2) and (6.3), the Fermi derivative component of the orthonormal basis in the direction of four-velocity u_α can be expressed as

$$u^\beta F_\beta e_\alpha = \omega_\alpha^\beta e_\beta. \quad (6.4)$$

It is worth noticing that $u^\beta F_\beta e_\alpha \neq 0$ for a rotating spacetime only. On another hand, let us note \mathcal{S} as the spin vector of a rigid rotator, such as a gyroscope, or the expected value of the spin operator for a particle. The change in spin \mathcal{S} with respect to proper time τ is expressed after expanding $u^\beta F_\beta \mathcal{S} = 0$ as follows

$$\frac{d\mathcal{S}^\alpha}{d\tau} = \omega_\beta^\alpha \mathcal{S}^\beta, \quad (6.5)$$

suggesting that the spin vector \mathcal{S} undergo precession with a certain frequency. To derive the needed quantity, we introduce the angular frequency

$$\omega_{ij} = \epsilon_{ijk}\omega^k, \quad (6.6)$$

where ϵ_{ijk} is the levi-civita tensor and ω^k represents the Lense-Thirring precession frequency. The angular velocity is described in terms of timelike Killing vector field K^α by the equation

$$\omega_{ij} = \frac{1}{\sqrt{-K^\alpha K_\alpha}} e_j^\beta K^\delta \nabla_\delta e_{i\beta}. \quad (6.7)$$

As a result the quantity Ω is given by

$$\Omega_\mu = \frac{1}{2\sqrt{-K^\alpha K_\alpha}} * (\bar{K} \wedge d\bar{K})_\mu, \quad (6.8)$$

where \wedge is the external product and $*$ is the Hodge operator [90]. The Lense-Thirring precession frequency for the spin vector \mathcal{S} can be expressed as follows

$$\Omega_\mu = \frac{1}{2\sqrt{-K^\alpha K_\alpha}} \mathcal{N}_\mu^{\nu\rho\sigma} K_\nu \partial_\rho K_\sigma, \quad (6.9)$$

where the canonical volume associated to the metric $g_{\mu\nu}$ is \mathcal{N} and $\mathcal{N}_\mu^{\nu\rho\sigma} = \frac{1}{4}\sqrt{-g}g_{\mu\alpha}\epsilon^{\alpha\nu\rho\sigma}$ with $\epsilon^{\alpha\nu\rho\sigma}$ being Levi-Civita symbol. The covariant form of the timelike Killing vector K^μ is $K_\mu = g_{\mu\nu}K^\nu$. In the case of a stationary spacetime, we can write $K^\mu = (1, 0, 0, 0)$ and $K_\mu = g_{\mu t}$ which yields the decomposition $K_\mu dx^\mu = g_{tt}dt + g_{ti}dx^i$ for a stationary test gyroscope. In this way, for a spacetime described by a general slowly rotating metric

$$ds^2 = -g_{tt}dt^2 + g_{rr}dr^2 + g_{\theta\theta}d\theta^2 + g_{\phi\phi}d\phi^2 - 2g_{t\phi}dtd\phi. \quad (6.10)$$

we obtain the following magnitude of the spin precession frequency

$$\Omega = \left(g_{\theta\theta} (\Omega_\theta)^2 + g_{rr} (\Omega_r)^2 \right)^{\frac{1}{2}}, \quad (6.11)$$

where one has used the following equations [88]

$$\Omega_\theta = \frac{g_{tt}}{2\sqrt{-g}} \left(\frac{g_{t\phi}}{g_{tt}} \right)_{,r}, \quad \Omega_r = \frac{g_{tt}}{2\sqrt{-g}} \left(\frac{g_{t\phi}}{g_{tt}} \right)_{,\theta}. \quad (6.12)$$

6.2 Graphics and results

In this part of the paper, we use the obtained results and apply them to our case which correspond to the acoustic black hole in the slowly rotating regime. Indeed, with the use of equations (3.24), (6.11) and (6.12), we find

$$\Omega_\theta = \frac{aM \sin(\theta) (\xi(r - 6M)(r - 2M) + r^2)}{r(2M - r) (r^2 - 2M\xi(r - 2M)) \sqrt{\Gamma}}, \quad (6.13)$$

$$\Omega_r = \frac{aM \sin(2\theta) (\xi(r - 2M)^2 + r^2)}{r^3 \sin(\theta) \sqrt{\Gamma}}, \quad (6.14)$$

where

$$\Gamma = r^4 - \frac{4a^2M^2 \sin^2(\theta) (\xi(r-2M)^2 + r^2)^2}{r(2M-r)(r^2 - 2M\xi(r-2M))}. \quad (6.15)$$

The final magnitude Ω is given by

$$\Omega = \left[-\frac{a^2M^2}{2r^2(2M-r)(\chi) \left(2a^2M^2(\cos(2\theta)-1)(\xi(r-2M)^2 + r^2)^2 + r^5(2M-r)(\chi) \right)} \right]^{\frac{1}{2}} \times \\ \left[(8M\xi^3(r-2M)^6 + \xi^2r^2(6M-r)(r-2M)^2(16M^2 - 22Mr + 5r^2) \right. \\ \left. + 2\xi r^4(2M-r)(4M-r)(6M-5r) + r^6(8M-5r) \right. \\ \left. + \cos(2\theta)(8M\xi^3(r-2M)^6 + \xi^2r^2(6M-r)(r-2M)^2(16M^2 - 10Mr + 3r^2) \right. \\ \left. + 2\xi r^4(2M-r)(24M^2 - 14Mr + 3r^2) + r^6(8M-3r) \right]^{\frac{1}{2}}, \quad (6.16)$$

where $\chi = r^2 - 2M\xi(r-2M)$. At the limit $\xi \rightarrow 0$, we obtain the following magnitude

$$\Omega = \sqrt{-\frac{a^2M^2(\cos(2\theta)(8M-3r) + 8M-5r)}{2(r^2(2M-r)(2a^2M^2(\cos(2\theta)-1) + r^3(2M-r)))}}. \quad (6.17)$$

This result matches perfectly the Kerr magnitude after some trigonometric rearrangements [88]. To reveal the behavior of such a quantity, we illustrate in figure (6) its behavior as a function of r for different values of the acoustic parameter ξ and the rotation a . From such a figure, we observe that the Kerr black hole magnitude is recovered when the case $\xi = 0$ is considered. In this case, the angular velocity decreases with the radius r since one moves away from the black hole. Near the event horizon, the spacetime is being dragged around the black hole causing the frame dragging effect to become extremely strong which leads to a very high value of the Lense Thirring precession. For the cases where $\xi \geq 4$, we remark that the value of Ω increases significantly around the acoustic radius r_{ac} for the extremal case, and around the inner and outer acoustic horizon in which $\xi > 4$. Such a result suggests that the frame-dragging effect is very strong in these regions. This could be interpreted by the twist of the spacetime that can be caused by the acoustic parameter ξ . Another important result arises from such illustrations. Precisely, at the equatorial plan ($\theta = \pi/2$), we have regions in which the the Lense-Thirring precession is null. These regions may be localised with the radial coordinate and are given by

$$r_{\Omega=0}^- = \frac{2M(2\xi - \sqrt{(\xi-3)\xi})}{\xi+1}, \quad (6.18)$$

$$r_{\Omega=0}^+ = \frac{2M(2\xi + \sqrt{(\xi-3)\xi})}{\xi+1}. \quad (6.19)$$

From the expression of the Ω given in equation (6.16), it can be seen that the angular velocity is null if $a = 0$. Such a case suggests that the Lense-Thirring effect is null for non rotating black hole. In our case, we have found that similar scenarios exist in the LTABH for values of the spin different than zero. Indeed, equations (6.18)-(6.19) show

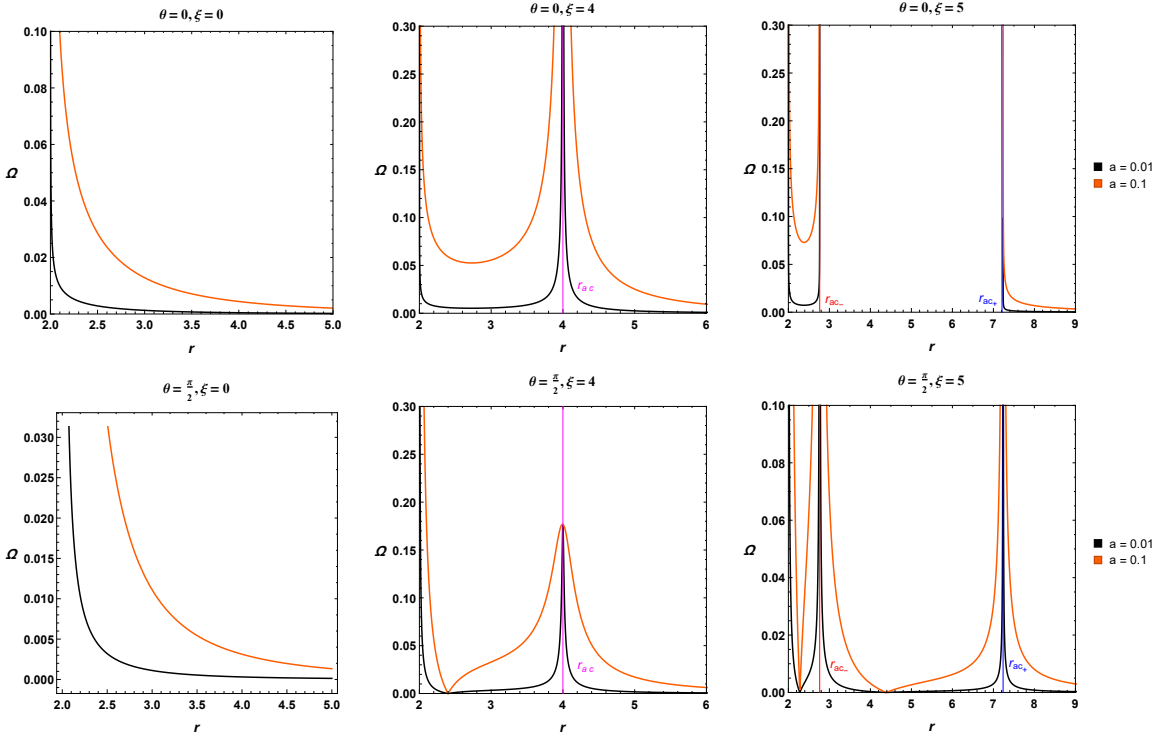


Figure 6: Lense-Thirring precession in a slowly rotating black hole for fixed $M = 1$. Left: Non-acoustic case. Middle: Extremal case of the acoustic black hole. Right: Acoustic black hole. We take $\theta = 0^\circ$ for the upper panels and $\theta = 90^\circ$ for the lower panels.

regions where the spacetime is not dragged by the black hole rotation parameter. This means that the particles orbits would not be subject of the precession occurring due to the frame dragging effect [91]. Such a result is essentially due to the acoustic parameter that cancels the rotating effect.

7 Deflection angle

The metric (3.24) describes a slowly rotating acoustic black hole. We begin by rewriting such a metric in the equatorial plane in order to get the required deflection angle of light. Indeed for $\theta = \frac{\pi}{2}$, we have

$$ds^2 = - \left[F(r) + 2a(1 - F(r)) \frac{d\phi}{dt} \right] dt^2 + \frac{dr^2}{F(r)} + r^2 d\phi^2. \quad (7.1)$$

The equations given in (5.7) can be used to compute the factor $\frac{d\phi}{dt}$ in this equation. The expression for such a quantity as a function of the impact parameter $b = \frac{L}{E}$, can be given by

$$\frac{d\phi}{dt} = \frac{F(r) + ba(1 - F(r))}{br^2 - a(1 - F(r))}. \quad (7.2)$$

Introducing the two new variables

$$dr_* = \frac{dr}{\sqrt{F(r) \left(F(r) + 2a(1 - F(r)) \frac{d\phi}{dt} \right)}}, \quad (7.3)$$

$$f(r_*) = \frac{r}{\sqrt{F(r) + 2a(1 - F(r)) \frac{d\phi}{dt}}}, \quad (7.4)$$

allows one to derive the optical metric on the equatorial plan for null geodesics ($ds^2 = 0$)

$$dt^2 = g_{mn}^{opt} dx^m dx^n = dr_*^2 + F(r_*)^2 d\phi^2. \quad (7.5)$$

We employ the Gauss-Bonnet theorem, which connects the optical geometry and topology, to compute the deflection angle. Such a theorem is written as

$$\iint_{D_R} K_G dS + \oint_{\partial D_R} k dt + \sum n_i = 2\pi\chi(D_R). \quad (7.6)$$

where the non-singular optical region D_R has a boundary ∂D_R , the geodesic curvature is k , the Gaussian optical curvature is represented by K_G and $\chi(D_R)$ is associated to the Euler characteristic. A geodesic curve, denoted as γ_R can be used to express the geodesic curvature as

$$k(\gamma_R) = |\nabla_{\gamma_R} \dot{\gamma}_R|. \quad (7.7)$$

Given that $\gamma_R = R = cte$ is verified by the geodesic γ_R [92], where R is the "geometrical size" of the region D_R , the radial component of $k(\gamma_R)$ becomes

$$(\nabla_{\gamma_R} \dot{\gamma}_R)^r = \dot{\gamma}_R^\phi + \partial_\phi \dot{\gamma}_R^r + \Gamma_{\phi\phi}^r \left(\dot{\gamma}_R^\phi \right)^2. \quad (7.8)$$

Following [92], the second term provides

$$\oint_{\partial D_R} k dt = \pi + \hat{\alpha}. \quad (7.9)$$

Furthermore, the jump angles α_S (source) and α_O (observer) are equal to $\frac{\pi}{2}$ when the geometrical size R of the optical region D_R approaches infinity. Given that the interior angles are $n_S = \pi - \alpha_S$ and $n_O = \pi - \alpha_O$ and by adopting the linear approach of the light ray, the deflection angle may be defined simply by

$$\hat{\alpha} = - \int_0^\pi \int_{\frac{b}{\sin \phi}}^\infty K_G dS, \quad (7.10)$$

where $dS \simeq r dr d\phi$. The Gaussian optical curvature can be computed in terms of the Ricci scalar by the following equation

$$K_G = \frac{\mathbf{R}}{2}, \quad (7.11)$$

which gives

$$K_G = \frac{18abM(\xi + 1)}{r^5} - \frac{2M(\xi + 1)}{r^3}. \quad (7.12)$$

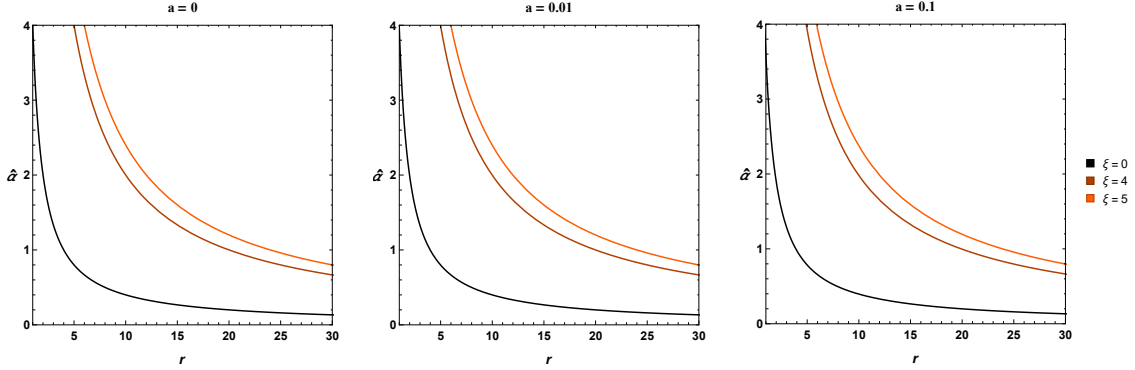


Figure 7: Deflection angle for different values of the acoustic parameter ξ and the spin a and fixed black hole mass ($M = 1$).

The deflection angles is finally expressed as

$$\hat{\alpha} = \frac{4M(\xi + 1)}{b} - \frac{4aM(\xi + 1)}{b^2} + \mathcal{O}(M^2, a^2), \quad (7.13)$$

where M higher orders are not included. At the limit $\xi \rightarrow 0$, the deflection angle (7.13) becomes

$$\hat{\alpha} \simeq \frac{4M}{b} \mp \frac{4aM}{b^2}, \quad (7.14)$$

where the \mp -branches would pertain to the pro-/retrograde motion. The obtained result matches precisely the LTBH black hole deflection of light [93]. To analyse the deflection of light by a slowly rotating acoustic black hole, we plot the associated behaviors as a function of the impact parameter b in figure (7) for different values of the acoustic parameter ξ and the spin a .

From such plots, we observe that the acoustic parameter ξ has a strong impact on the deflection of light. Such behaviour, should indeed be expected from the shadow study of the previous section. By comparing the different curves, we notice that the light is strongly deflected for the values $\xi \geq 4$. Considering the rotation coded in the parameter a , only small deviations occur suggesting that the acoustic parameter might have stronger influence than the rotation of the black hole it self.

8 Conclusions

In this paper, we have reviewed the Lense-Thirring acoustic black hole (LTABH), and probed its near horizon features. We showed that the LTABH exhibit similarities and differences with respect to its gravitational analogue, the Lense-Thirring Black Hole (LTBH). For what concerns the metric function, we showed that the rotation parameter does not affect its roots, as instead does the acoustic parameter ξ , which gives rise to radii depending on its value. More precisely, we found the existence of an inner acoustic horizon r_{ac-} and of an outer acoustic horizon r_{ac+} when $\xi > 4$. The extremal regime of the LTABH is reached for $\xi = 4$, implying $r_{ac-} = r_{ac+} = 4M$. Based on these results, also by means of various

graphics, we have characterized the metric function of the LTABH, and split its spacetime into four regions.

Furthermore, we have defined an effective potential, and studied its critical points (in particular, its maxima). We showed that the effective potential of the LTABH is characterized by two maxima, which are associated to the photon sphere (of radius r_{ps}) and to the acoustic sphere (of radius r_{as}), respectively; such radii have been placed and investigated carefully, as functions of the acoustic parameter ξ and of the rotation parameter a . We have been therefore able to conclude the LTABH is characterized by two shadows : the *optical shadow*, denoted as R_s , and the *acoustic shadow* denoted as R_{as} . In this context, the limit $\xi \rightarrow 0$ has provided an important consistency check of our approach.

By varying the rotation parameter a , we noticed that it strongly affects the radius of the optical shadow, while it has less impact onto the radius of the acoustic shadow. This fact has also been observed on the shapes of the shadows themselves : in fact, by varying a , we have observed that the acoustic shadow retains its circular shape, whereas the optical shadow is shifted rightward. On the other hand, we established that the acoustic parameter ξ is responsible for the size of the shadows; all in all, one should expect larger shadows when it comes to an acoustic black hole. All of such results have also been confirmed by the analyses of the distortions $\delta_{s/as}$, as well as of the shadow radii $R_{s/as}$.

By deriving the magnitude of the precession frequency Ω , we also have investigated the frame dragging effect in the LTABH. Of course, our results perfectly match the Kerr magnitude in the limit $\xi \rightarrow 0$. To shed light on the frame dragging, we have set up a parametric description and varied the relevant parameters accordingly : this allowed us to provide substantial evidence that Ω significantly increases near the acoustic horizons, both in the extremal case and in the non-extremal one; this is an indication that the frame dragging becomes important near such regions. Moreover, it has been shown that Ω becomes null in some radial regions at the equatorial plan; such regions have analytically been determined, and we were able to find that in some regions of the parameter space the orbits of probe particles would not be affected by the frame dragging. Interestingly, this insensitivity has been traced back to the presence of the acoustic parameter ξ . *Last but not least*, we have derived and analyzed the deflection of light by the LTABH, conforming and detailing the results obtained in the shadow analysis.

As of today, acoustic black holes have been the object of a vast variety of studies, both at the theoretical and experimental level. We share the belief, widely spread within the scientific community, that a deeper understanding of such black holes may importantly contribute to formulate models of more and more realistic astrophysical black holes. We can therefore reasonably state that the rotating class of acoustic black holes, to which the LTABH introduced in this paper belongs, warrants and deserves further investigation (for instance, the construction of an analogue-Kerr black hole still remains an open issue). We leave such intriguing tasks to future endeavours.

A On the placement of critical radii

Further investigation could be carried regarding the LTABH who's spacetime is described by the metric of equation (3.24). Indeed, we have seen that such a spacetime strongly depend on the value of the acoustic parameter ξ . While the horizon radius is always equal to $2M$, distinctions are also present. For convenience, we use the following notations

$$r_1 := r_{ps}, \quad R_s(r_1) = R_s(r_{ps}) := R_s, \quad r_2 := r_{as}, \quad R_s(r_2) = R_s(r_{as}) := R_{as}. \quad (\text{A.1})$$

In what follows, we discuss and picture each case for a better understanding of such important spacetime distribution. First, we have the non acoustic case ($\xi = 0$) in which the inner and outer acoustic horizon vanishes. The relevant radii for this particular case are given in table (3).

Table 3: Critical radii values for the non acoustic case. We take $M = 1$, $E = \mathcal{K} = 1$ and $L = 20$.

ξ	r_H	a	r_{ps}	R_s
0	2	0	3	5.196
		0.1	3.03	5.248
		0.2	3.06	5.3

Thus, we remark that for such a case the rotation parameter a increases the photon sphere r_{ps} and the shadow radius R_s . The extremal acoustic case in which $\xi = 4$ is characterized by a horizon and an acoustic radius. Both of these quantities does not depend on the rotating parameter a . The other relevant quantities are provided in table (4).

Table 4: Critical radii values for the extremal acoustic case. We take $M = 1$, $E = \mathcal{K} = 1$ and $L = 20$.

ξ	r_H	r_{ac}	a	r_{ps}	r_{as}	R_s	R_{as}
4	2	4	0	2.299	8.7	8.62	18.35
			0.1	2.31	8.92	9.24	18.67
			0.2	2.32	9.13	10	18.98

It is clear from such a table that all the critical radii values increases with the rotating parameter a . By comparing these values with the case where $\xi = 0$, it is clear that the impact of ξ might be different on each quantity. For instance, we remark that the photon sphere r_{ps} decreased while the shadow radius R_s increased. In the case where $\xi \geq 4$, there is an inner and outer acoustic horizon which are r_{ac_-} and r_{ac_+} respectively. In table (5), we specify the relevant radii for different values of the rotating parameter a .

Table 5: Critical radii values for the acoustic case. We take $M = 1$, $E = \mathcal{K} = 1$ and $L = 20$.

ξ	r_H	r_{ac_-}	r_{ac_+}	a	r_{ps}	r_{as}	R_s	R_{as}
5	2	2.77	7.24	0	2.23	12.05	9.47	23.78
				0.1	2.24	12.26	10.39	24.12
				0.2	2.25	12.47	11.63	24.47

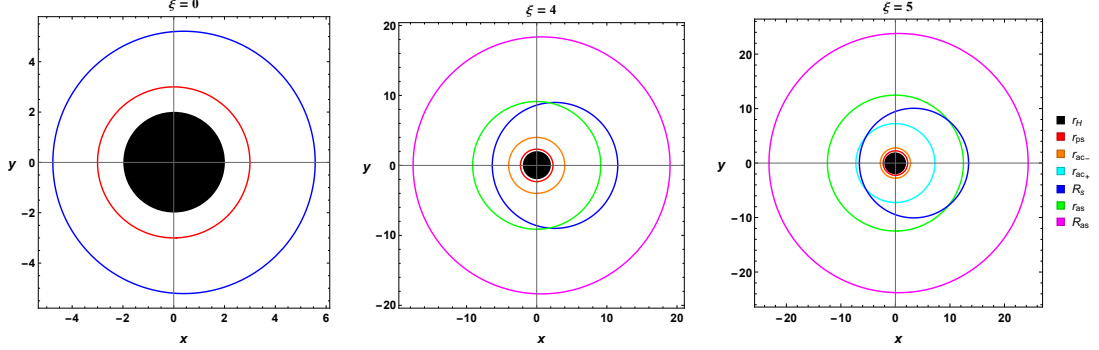


Figure 8: Illustration of the critical radii for different values of the acoustic parameter ξ . Left: Non acoustic case. Middle: Extremal case of the acoustic black hole. Right: Acoustic black hole. We take $a = 0.2$, $M = 1$, $E = \mathcal{K} = 1$ and $L = 20$.

From such a table, we can confirm that the photon sphere r_{ps} decreases with the increase of the parameter ξ while all the other quantities increase. The impact of the rotating parameter a is the same for all quantities as it can be observed from the tables. It can be remarked that the photon sphere r_{ps} has decreased more in size compared to the extremal acoustic case while the other quantities have increased. In figure 8, we report each of the critical radii for all the cases discussed above. It is worth noting that the interaction Photon-Phonon is not taken into account in this paper; we leave the investigation of such an interaction for further future work.

B The matrix $\mathcal{G}_{\mu\nu}$

The explicit $\mathcal{G}_{\mu\nu}$ matrix is

$$\mathcal{G}_{\mu\nu} = \begin{pmatrix} \mathcal{G}_{tt} & \mathcal{G}_{tr} & \mathcal{G}_{t\theta} & \mathcal{G}_{t\phi} \\ \mathcal{G}_{rt} & \mathcal{G}_{rr} & \mathcal{G}_{r\theta} & \mathcal{G}_{r\phi} \\ \mathcal{G}_{\theta t} & \mathcal{G}_{\theta r} & \mathcal{G}_{\theta\theta} & \mathcal{G}_{\theta\phi} \\ \mathcal{G}_{\phi t} & \mathcal{G}_{\phi r} & \mathcal{G}_{\phi\theta} & \mathcal{G}_{\phi\phi} \end{pmatrix}, \quad (\text{B.1})$$

with

$$\mathcal{G}_{tt} = \frac{c_s}{\sqrt{c_s^2 - v_\alpha v^\alpha}} g_{tt} (c_s^2 - v_i v^i), \quad (\text{B.2})$$

$$\mathcal{G}_{tr} = \frac{c_s}{\sqrt{c_s^2 - v_\alpha v^\alpha}} (-v_t v_r + g_{tr} (c_s^2 - v_i v^i)), \quad (\text{B.3})$$

$$\mathcal{G}_{t\theta} = \frac{c_s}{\sqrt{c_s^2 - v_\alpha v^\alpha}} (-v_t v_\theta + g_{t\theta} (c_s^2 - v_i v^i)), \quad (\text{B.4})$$

$$\mathcal{G}_{t\phi} = \frac{c_s}{\sqrt{c_s^2 - v_\alpha v^\alpha}} (-v_t v_\phi + g_{t\phi} (c_s^2 - v_i v^i)), \quad (\text{B.5})$$

$$\mathcal{G}_{rt} = \frac{c_s}{\sqrt{c_s^2 - v_\alpha v^\alpha}} (-v_r v_t + g_{rt} (c_s^2 - v_i v^i)), \quad (\text{B.6})$$

$$\mathcal{G}_{rr} = \frac{c_s}{\sqrt{c_s^2 - v_\alpha v^\alpha}} (g_{rr} (c_s^2 - v_\alpha v^\alpha) + v_r v_r), \quad (\text{B.7})$$

$$\mathcal{G}_{r\theta} = \frac{c_s}{\sqrt{c_s^2 - v_\alpha v^\alpha}} (g_{r\theta}(c_s^2 - v_\alpha v^\alpha) + v_r v_\theta), \quad (\text{B.8})$$

$$\mathcal{G}_{r\phi} = \frac{c_s}{\sqrt{c_s^2 - v_\alpha v^\alpha}} (g_{r\phi}(c_s^2 - v_\alpha v^\alpha) + v_r v_\phi), \quad (\text{B.9})$$

$$\mathcal{G}_{\theta t} = \frac{c_s}{\sqrt{c_s^2 - v_\alpha v^\alpha}} (-v_\theta v_t + g_{\theta t}(c_s^2 - v_t v^t)), \quad (\text{B.10})$$

$$\mathcal{G}_{\theta r} = \frac{c_s}{\sqrt{c_s^2 - v_\alpha v^\alpha}} (g_{\theta r}(c_s^2 - v_\alpha v^\alpha) + v_\theta v_r), \quad (\text{B.11})$$

$$\mathcal{G}_{\theta\theta} = \frac{c_s}{\sqrt{c_s^2 - v_\alpha v^\alpha}} (g_{\theta\theta}(c_s^2 - v_\alpha v^\alpha) + v_\theta v_\theta), \quad (\text{B.12})$$

$$\mathcal{G}_{\theta\phi} = \frac{c_s}{\sqrt{c_s^2 - v_\alpha v^\alpha}} (g_{\theta\phi}(c_s^2 - v_\alpha v^\alpha) + v_\theta v_\phi), \quad (\text{B.13})$$

$$\mathcal{G}_{\phi t} = \frac{c_s}{\sqrt{c_s^2 - v_\alpha v^\alpha}} (-v_\phi v_t + g_{\phi t}(c_s^2 - v_t v^t)), \quad (\text{B.14})$$

$$\mathcal{G}_{\phi r} = \frac{c_s}{\sqrt{c_s^2 - v_\alpha v^\alpha}} (g_{\phi r}(c_s^2 - v_\alpha v^\alpha) + v_\phi v_r), \quad (\text{B.15})$$

$$\mathcal{G}_{\phi\theta} = \frac{c_s}{\sqrt{c_s^2 - v_\alpha v^\alpha}} (g_{\phi\theta}(c_s^2 - v_\alpha v^\alpha) + v_\phi v_\theta), \quad (\text{B.16})$$

$$\mathcal{G}_{\phi\phi} = \frac{c_s}{\sqrt{c_s^2 - v_\alpha v^\alpha}} (g_{\phi\phi}(c_s^2 - v_\alpha v^\alpha) + v_\phi v_\phi). \quad (\text{B.17})$$

References

- [1] A. Einstein, *Die Grundlagen der allgemeinen, Relativitats-teorie*, Annale der Physic, **49**, 1916, 769.
- [2] J. R. Oppenheimer, H. Snyder, *On continued gravitational contraction*, Physical Review, **56**, 1939, 455.
- [3] M. Volonteri, *The formation and evolution of massive black holes*, Science, **337**, 2012, 544-547.
- [4] V. Bozza, *Gravitational lensing by black holes*, General Relativity and Gravitation, **42**, 2010, 2269-2300.
- [5] V. Bozza, S. Capozziello, G. Iovane, G. Scarpetta, *Strong field limit of black hole gravitational lensing*, General Relativity and Gravitation, **33**, 2001, 1535-1548.
- [6] K. S. Virbhadra, G. F. Ellis, *Gravitational lensing by naked singularities*, Physical Review D, **65**, 2002, 103004.
- [7] K. Jusufi, A. Övgün, J. Saavedra, Y. Vásquez, P. A. Gonzalez, *Deflection of light by rotating regular black holes using the Gauss-Bonnet theorem*, Physical Review D, **97**, 2018, 124024.
- [8] R. Kumar, S. G. Ghosh, A. Wang, *Shadow cast and deflection of light by charged rotating regular black holes*, Physical Review D, **100**, 2019, 124024.
- [9] A. Belhaj, M. Benali, A. El Balali, H. El Moumni, S. E. Ennadifi, *Deflection angle and shadow behaviors of quintessential black holes in arbitrary dimensions*, Classical and Quantum Gravity, **37**, 2020, 215004.
- [10] A. El Balali, M. Benali, M. Oualaid, *Deflection angle and shadow of slowly rotating black holes in galactic nuclei*, General Relativity and Gravitation, **56**, 2024, 21.

- [11] V. Perlick, *Gravitational lensing from a spacetime perspective*, Living reviews in relativity **7**, 2004, 1-117.
- [12] V. Perlick, O. Y. Tsupko, *Calculating black hole shadows: Review of analytical studies*, Physics Reports **947**, 2022, 1-39.
- [13] Z. Younsi, A. Zhidenko, L. Rezzolla, R. Konoplya, Y. Mizuno, *New method for shadow calculations: Application to parametrized axisymmetric black holes*, Physical Review D, **94**, 2016, 084025.
- [14] Y. Mizuno, Z. Younsi, C. M. Fromm, O. Porth, M. De Laurentis, H. Olivares, L. Rezzolla, *The current ability to test theories of gravity with black hole shadows*, Nature Astronomy, **2**, 2018, 585-590.
- [15] A. Belhaj, M. Benali, A. El Balali, W. El Hadri, H. El Moumni, E. Torrente-Lujan, *Black hole shadows in M-theory scenarios*, International Journal of Modern Physics D, **30**, 2021, 2150026.
- [16] A. El Balali, *Quantum Schwarzschild Black Hole Optical Aspects*, Gravitation and Cosmology, **30**, 2024, 71-84.
- [17] R. A. Konoplya, *Shadow of a black hole surrounded by dark matter*, Physics Letters B **795**, 2019, 1-6.
- [18] J. D. Bekenstein, *Black holes and the second law*, In JACOB BEKENSTEIN: The Conservative Revolutionary, 2020, pp. 303-306.
- [19] J. D. Bekenstein, *Black hole thermodynamics*, Physics Today, **33**, 1980, 24-31.
- [20] J. D. Bekenstein, *Black holes and entropy*, Physical Review D **7**, 1973, 2333.
- [21] S. W. Hawking, *Black hole explosions?*, Nature, **248**, 1974, 30-31.
- [22] S. W. Hawking, *Particle creation by black holes*, Communications in mathematical physics, **43**, 1975, 199-220.
- [23] S. Carlip, *Black hole thermodynamics*, International Journal of Modern Physics D, **23**, 2014, 1430023.
- [24] A. Belhaj, A. El Balali, W. El Hadri, H. El Moumni, M. B. Sedra, *Dark energy effects on charged and rotating black holes*, The European Physical Journal Plus, **134**, 2019, 422.
- [25] D. N. Page, *Hawking radiation and black hole thermodynamics*, New Journal of Physics, **7**, 2005, 203.
- [26] A. Perez, *Black holes in loop quantum gravity*, Reports on Progress in Physics, **80**, 2017, 126901.
- [27] P. Nicolini, *Noncommutative black holes, the final appeal to quantum gravity: a review*, International Journal of Modern Physics A, **24**, 2009, 1229-1308.
- [28] C. Rovelli, *Black hole entropy from loop quantum gravity*, Physical Review Letters, **77**, 1996, 3288.
- [29] C. Kiefer, *Why quantum gravity?*, Approaches to Fundamental Physics: An Assessment of Current Theoretical Ideas. Berlin, Heidelberg: Springer Berlin Heidelberg, 2007, 123-130.
- [30] M. Maggiore, *A generalized uncertainty principle in quantum gravity*, Physics Letters B, **304**, 1993, 65-69.

- [31] B. P. Abbott et al, LIGO Scientific, Virgo collaboration, *Properties of the Binary Black Hole Merger GW150914*, Phys. Rev. Lett. **116**, 2016 241102.
- [32] K. Akiyama et al., Event Horizon Telescope collaboration, *First M87 Event Horizon Telescope Results. I. The Shadow of the Supermassive Black Hole*, Astrophys. J. Lett. **875**, 2019, L1.
- [33] K. Akiyama et al., Event Horizon Telescope collaboration, *First M87 Event Horizon Telescope Results. II. Array and Instrumentation*, Astrophys. J. Lett. **875**, 2019, L2.
- [34] K. Akiyama et al., Event Horizon Telescope collaboration, *First M87 Event Horizon Telescope Results. III. Data Processing and Calibration*, Astrophys. J. Lett. **875**, 2019, L3.
- [35] K. Akiyama et al., Event Horizon Telescope collaboration, *First M87 Event Horizon Telescope Results. IV. Imaging the Central Supermassive Black Hole*, Astrophys. J. Lett. **875**, 2019, L4.
- [36] K. Akiyama et al., Event Horizon Telescope collaboration, *First M87 Event Horizon Telescope Results. V. Physical Origin of the Asymmetric Ring*, Astrophys. J. Lett. **875**, 2019, L5.
- [37] K. Akiyama et al., Event Horizon Telescope collaboration, *First M87 Event Horizon Telescope Results. VI. The Shadow and Mass of the Central Black Hole*, Astrophys. J. Lett. **875**, 2019, L6.
- [38] K. Akiyama, et al, The Event Horizon Telescope Collaboration, *First M87 event horizon telescope results. VII. Polarization of the ring*, Astrophys. J. Lett. **910**, 2021, p. L12.
- [39] K. Akiyama, et al, The Event Horizon Telescope Collaboration, *First M87 event horizon telescope results. VIII. Magnetic field structure near the event horizon*, Astrophys. J. Lett. **910**, 2021, p. L13.
- [40] W. G. Unruh, *Experimental black hole evaporation*, Phys. Rev. Lett. **46**, 1981, 1351.
- [41] X. H. Ge, S. J. Sin, *Acoustic black holes for relativistic fluids*, JHEP, **06**, 2010, 1-16.
- [42] M. Visser, *Acoustic black holes: Horizons, ergospheres, and Hawking radiation*, Class. Quant. Grav. **15**, 1998, 1767-1791.
- [43] U. R. Fischer, R. Schützhold, *Quantum simulation of cosmic inflation in two-component Bose-Einstein condensates*, Physical Review A—Atomic, Molecular, and Optical Physics **70**, 2004, 063615.
- [44] P. O. Fedichev, U. R. Fischer, *Gibbons-Hawking Effect in the Sonic de Sitter Space-Time of an Expanding Bose-Einstein-Condensed Gas*, Physical review letters, **91**, 2003, 240407.
- [45] R. Schutzhold, W.G. Unruh, *Gravity wave analogs of black holes*, Phys. Rev. D **66**, 2002, 044019.
- [46] G. Rousseaux, C. Mathis, P. Maissa, T.G. Philbin, U. Leonhardt, *Observation of negative phase velocity waves in a water tank: A classical analogue to the Hawking effect?*, New J. Phys. **10**, 2008, 053015.
- [47] U. Leonhardt, P. Piwnicki, *Relativistic effects of light in moving media with extremely low group velocity*, Phys. Rev. Lett. **84**, 2000, 822.
- [48] U. Leonhardt, *A laboratory analogue of the event horizon using slow light in an atomic medium*, Nature **415**, 2002, 406.

[49] W.G. Unruh, R. Schutzhold, *On slow light as a black hole analogue*, Phys. Rev. D **68**, 2003, 024008.

[50] T G. Philbin, C. Kuklewicz, S. Robertson, S Hill, F. Konig, U. Leonhardt, *Fiber-optical analogue of the event horizon*, Science **319**, 2008, 1367.

[51] R. Schutzhold, W. G. Unruh, *Hawking radiation in an electro-magnetic wave-guide?*, Phys. Rev. Lett. **95**, 2005, 031301.

[52] M. Novello, M. Visser and G. Volovik, *Artificial black holes*, World Scientific, Singapore Republic of Singapore, 2002.

[53] L. J. Garay, J. R. Anglin, J. I. Cirac, P. Zoller, *Black holes in Bose-Einstein condensates*, Phys. Rev. Lett. **85**, 2000, 4643.

[54] S. Giovanazzi, *Hawking radiation in sonic black holes*, Phys. Rev. Lett. **94**, 2005, 061302.

[55] C. Barcelo, S. Liberati, M. Visser, *Analogue gravity*, Living reviews in relativity **14**, 2011, 1-159.

[56] J. R. Muñoz de Nova, K. Golubkov, V. I. Kolobov, J. Steinhauer, *Observation of thermal Hawking radiation and its temperature in an analogue black hole*, Nature **569**, 2019, 688-691.

[57] M. Isoard, N. Pavloff, *Departing from thermality of analogue Hawking radiation in a Bose-Einstein condensate*, Phys. Rev. Lett. **124**, 2020, 060401.

[58] O. Lahav, A. Itah, A. Blumkin, C. Gordon, J. Steinhauer, *Realization of a sonic black hole analog in a Bose-Einstein condensate*, Phys. Rev. Lett. **105**, 2010, 240401.

[59] H. H. Zhao, G. L. Li, L. C. Zhang, *Generalized uncertainty principle and entropy of three-dimensional rotating acoustic black hole*, Phys. Lett. A **376**, 2012, 2348-2351

[60] M. A. Anacleto, F. A. Brito, E. Passos, W. P. Santos, *The entropy of the noncommutative acoustic black hole based on generalized uncertainty principle*, Phys. Lett. B **737**, 2014, 6-11.

[61] M. A. Anacleto, F. A. Brito, G. C. Luna, E. Passos and J. Spinelly, *Quantum-corrected finite entropy of noncommutative acoustic black holes*, Annals Phys. **362** (2015), 436-448.

[62] M. A. Anacleto, I. G. Salako, F. A. Brito, E. Passos, *The entropy of an acoustic black hole in neo-Newtonian theory*, Int. J. Mod. Phys. A **33**, 2018, 1850185.

[63] M. A. Anacleto, F. A. Brito, C. V. Garcia, G. C. Luna, E. Passos, *Quantum-corrected rotating acoustic black holes in Lorentz-violating background*, Phys. Rev. D **100**, 2019, 105005.

[64] B. Zhang, *Thermodynamics of acoustic black holes in two dimensions*, Adv. High Energy Phys. 2016, 5710625.

[65] S. Y. Chä, U. R. Fischer, *Probing the scale invariance of the inflationary power spectrum in expanding quasi-two-dimensional dipolar condensates*, Physical review letters **118**, 2017, 130404.

[66] M. Rinaldi, *The entropy of an acoustic black hole in Bose-Einstein condensates*, Phys. Rev. D **84**, 2011, 124009.

[67] S. Giovanazzi, *Entanglement Entropy and Mutual Information Production Rates in Acoustic Black Holes*, Phys. Rev. Lett. **106**, 2011, 011302.

[68] J. Steinhauer, *Measuring the entanglement of analogue Hawking radiation by the density-density correlation function*, Phys. Rev. D **92**, 2015, 024043.

[69] X. H. Ge, M. Nakahara, S. J. Sin, Y. Tian, S. F. Wu, *Acoustic black holes in curved spacetime and the emergence of analogue Minkowski spacetime*, Phys. Rev. D **99**, 2019, 104047.

[70] C. Yu, J. R. Sun, *Note on acoustic black holes from black D3-brane*, Int. J. Mod. Phys. D **28**, 2019, 1950095.

[71] M. A. Anacleto, F. A. Brito, E. Passos, *Acoustic Black Holes from Abelian Higgs Model with Lorentz Symmetry Breaking*, Phys. Lett. B **694**, 2011, 149-157.

[72] H. Guo, H. Liu, X. M. Kuang, B. Wang, *Acoustic black hole in Schwarzschild spacetime: Quasinormal modes, analogous Hawking radiation, and shadows*, Physical Review D, **102**, 2020, 124019.

[73] J. A. V. Campos, M. A. Anacleto, F. A. Brito, E. Passos, *Absorption, scattering, quasinormal modes and shadow by canonical acoustic black holes in Lorentz-violating background*, General Relativity and Gravitation, **56**, 2024, 74.

[74] C. K. Qiao, M. Zhou, *The gravitational bending of acoustic Schwarzschild black hole*, The European Physical Journal C, **83**, 2023, 271.

[75] N. U. Molla, U. Debnath, *Gravitational lensing of acoustic charged black holes*, The Astrophysical Journal, **947**, 2023, 14.

[76] H. S. Vieira, K. Destounis, K. D. Kokkotas, *Slowly-rotating curved acoustic black holes: Quasinormal modes, Hawking-Unruh radiation, and quasibound states* Physical Review D **105**, 2022, 045015.

[77] V. Moncrief, *Stability of stationary, spherical accretion onto a Schwarzschild black hole*, Astrophys. J. **235**, 1980, 1038.

[78] T. K. Das, *Analogue Hawking radiation from astrophysical black-hole accretion*, Class. Quant. Grav. **21**, 2004, 5253.

[79] T. K. Das, *Transonic black hole accretion as analogue system*, arXiv preprint gr-qc/0411006.

[80] H. Abraham, N. Bilic, T. K. Das, *Acoustic horizons in axially symmetric relativistic accretion*, Classical and Quantum Gravity, **23**, 2006, 2371.

[81] L. Berezhiani, J. Khouri, *Theory of dark matter superfluidity*, Physical Review D, **92**, 2015, 103510.

[82] J. Baines, T. Berry, A. Simpson, M. Visser, *Painlevé–Gullstrand form of the Lense–Thirring spacetime*, Universe, **7**, 2021, 105.

[83] R. Ling, H. Guo, H. Liu, X. M. Kuang, B. Wang, *Shadow and near-horizon characteristics of the acoustic charged black hole in curved spacetime*, Physical Review D **104**, 2021, 104003.

[84] B. Carter, *Global structure of the Kerr family of gravitational fields*, Phys. Rev. **174**, 1968, 1559.

[85] S. Vazquez, E. P. Esteban, *Strong field gravitational lensing by a Kerr black hole*, Nuovo Cim.B **119**, 2004, 489.

[86] J. Lense, H. Thirring, *On the influence of the proper rotation of a central body on the motion of the planets and the moon, according to Einstein's theory of gravitation*, Zeitschrift für Physik **19**, 1918, 47.

[87] L. I. Schiff, *Possible new experimental test of general relativity theory*, Physical Review Letters, **4**, 1960, 215.

- [88] P. Bambhaniya, J. V. Trivedi, D. Dey, P. S. Joshi, A. B. Joshi, *Lense Thirring effect and precession of timelike geodesics in slowly rotating black hole and naked singularity spacetimes*, Physics of the Dark Universe, **40**, 2023, 101215.
- [89] C. Chakraborty, P. Kocherlakota, M. Patil, S. Bhattacharyya, P. S. Joshi, A. Królak, *Distinguishing Kerr naked singularities and black holes using the spin precession of a test gyro in strong gravitational fields*, Physical Review D **95**, 2017, 084024.
- [90] M. H. Wu, H. Guo, X. M. Kuang, *Precession and Lense-Thirring effect of hairy Kerr spacetimes*, Physical Review D, **107**, 2023, 064033.
- [91] C. Chakraborty, P. Kocherlakota, P. S. Joshi, *Spin precession in a black hole and naked singularity spacetimes*, Physical Review D, **95**, 2017, 044006.
- [92] G.W. Gibbons, M. C. Werner, *Applications of the Gauss-Bonnet theorem to gravitational lensing*, Classical and Quantum Gravity, **25**, 2008, 235009.
- [93] T. Zhu, Q. Wu, M. Jamil, K. Jusufi, *Shadows and deflection angle of charged and slowly rotating black holes in Einstein- \mathcal{A} ether theory*, Physical Review D, **100**, 2019, 044055.